# Temperature-dependent cyclic deformation behavior of CoCrFeMnNi high-entropy alloy

Kaiju Lu[1]*, Ankur Chauhan[1,2], Dimitri Litvinov[1], Jarir Aktaa[1]

[1]Institute for Applied Materials, Karlsruhe Institute of Technology (KIT), Hermann-von-Helmholtz-Platz 1, 76344, Eggenstein-Leopoldshafen, Germany

[2]Department of Materials Engineering, Indian Institute of Science, Bengaluru, 560012, Karnataka, India

Email: *kaiju.lu@kit.edu; kaiju.lu@hotmail.com

## Abstract

We compare the low-cycle fatigue behavior of a CoCrFeMnNi high-entropy alloy at room-temperature (RT) and 550 °C. The cyclic response at 550 °C manifests no cyclic softening, presence of serrated flow and reduced fatigue life compared to that at RT. Microstructural investigations show that distinctly from the dominating wavy slip at RT, dislocations planar slip complements wavy slip at 550 °C. The unexpected planar slip at 550 °C is ascribed to the increase of stacking fault width, likely due to Suzuki segregation. Furthermore, dislocation slip mode evolution with both strain amplitude and cycle number at 550 °C is revealed.

**Keywords:** High-entropy alloy; Fatigue; Dislocation; Transmission electron microscopy (TEM); Temperature.

## 1. Introduction

Recently, unceasing endeavors have been exerted in characterizing the low-cycle fatigue (LCF) behavior of equiatomic CoCrFeMnNi high-entropy alloy (HEA) with face-centered cubic (FCC) crystal structure [1-5]. These investigations were mostly restricted to understanding its room temperature (RT) behavior [1-5]. However, in high-temperature engineering applications (*e.g.*, power plants and nuclear reactors), structural components and/or materials are inevitably subjected to thermo-mechanical cyclic loads. Hence, if such applications are to be foreseen for HEAs, the understanding of their cyclic response at elevated temperatures becomes mandatory. So far, only one known study [6] has uncovered the LCF behavior of CoCrFeMnNi at an elevated temperature (*i.e.*, 550 °C, which is above $0.5T_m$ and lies within the proposed operating temperature range of advanced power plants and nuclear reactors [7-9]). Note that, the melting temperature $T_m$ of CoCrFeMnNi alloy lies in the range of 1523 K to 1553 K [10].

It is well-established that the LCF behavior of a ductile metallic material is closely related to the underlying deformation mechanisms, especially the evolution of dislocation structures [1-5, 11-14]. For instance, at RT, the dislocation structures and corresponding slip mode of CoCrFeMnNi alter with both strain amplitude and cycle number [5]. Since preliminary LCF investigations at 550 °C were limited to characterizing the evolution of dislocation density [6], it still remains unclear how the slip mode and dislocation structures evolve with strain amplitude as well as cycle number at elevated temperatures.

Furthermore, it is also important to understand the temperature influence on the CoCrFeMnNi's deformation behavior, which until now has only been investigated *via* tension, compression [15, 16], and creep tests [17]. For instance, Otto et al. [15] investigated the temperature influence on the tensile properties and underlying deformation mechanisms of CoCrFeMnNi. It has been revealed that the initial plastic strain (*i.e.*, up to ~ 2%) from 77 K to 873 K in CoCrFeMnNi is accommodated by planar slip of partial dislocations [15]. This observation suggested the prevalence of planar slip upon cycling CoCrFeMnNi at initial cycles [5]. Despite these efforts to understand the temperature influence on the monotonic deformation mechanisms [15-17], there exists a knowledge gap regarding its influence on the cyclic deformation mechanisms of CoCrFeMnNi.

Consequently, this work seeks to deepen the understanding of the cyclic deformation mechanisms of CoCrFeMnNi HEA at an elevated temperature (*i.e.*, 550 °C). Furthermore, this work aims at providing first insights into temperature influence on the HEA's cyclic deformation behavior.

## 2. Experimental details

The investigated equiatomic CoCrFeMnNi was synthesized by arc melting followed by drop-casting. The as-cast ingots were then homogenized at 1200 °C for 72 h followed by water quenching and rotary swaging. The LCF specimens, with a gauge diameter of 2 mm and a gauge length of 7.6 mm, were then fabricated from the rotary swaged material parallel to the longitudinal direction. Before fatigue tests, LCF specimens were recrystallized by annealing at 800 °C for 1 hour. Briefly, the as-recrystallized microstructure manifests an average grain size of ~ (6 ± 3) μm and low density of dislocations. For more details on the initial microstructure of the material, see Refs. [3, 6].

Fully-reversed pull-to-push LCF-tests were carried out under different strain amplitudes with a nominal strain rate of $3\times10^{-3}$ $s^{-1}$ at both RT and 550 °C. In specific, at RT, the applied strain amplitudes include 0.3%, 0.5%, 0.6% and 0.7% (two tests per condition); whereas, at 550 °C, it is 0.2%, 0.3%, 0.4%, 0.5%, 0.75%, and 0.8% (one test per condition, due to limited amount of material). These strain amplitudes were chosen to ensure that the lifetime is within the LCF regime. It should be noted that, the cyclic stress response and lifetime of CoCrFeMnNi at RT and 550 °C, previously reported in Refs. [3] and [6], are reanalyzed with emphasis on exploring the underlying temperature influence. Despite the limited number of test at each condition, the scatters in cyclic stress response and lifetime are reasonable (see later Results section).

To understand deformation mechanisms, the post-fractured microstructure was characterized by electron backscatter diffraction (EBSD) and transmission electron microscopy (TEM). EBSD investigations were carried out on an FEI 200 Dual-Beam SEM/FIB equipped with an HKL EBSD detector (for the employed parameters, see Ref. [6]). The acquired EBSD data were post-processed by EDAX's OIM software to obtain kernel average misorientation (KAM) maps. As KAM considers only misorientations in a small local neighborhood within a grain, it also provides a good estimation of the local

geometrically necessary dislocation (GND) density [18]. In specific, higher KAM values correspond to higher local misorientations (*i.e.*, higher GND density) and vice versa.

For TEM investigations, an FEI Tecnai F20 TEM microscope was employed operating at an accelerating voltage of 200 kV. For EBSD and TEM samples preparation, conventional procedures including mechanical grinding, polishing and/or twin-jet electro-polishing were employed, see Ref. [6].

## 3. Results

To seek the difference in the cyclic response at different temperatures, Fig. 1a presents the peak tensile stress *versus* normalized number of cycles curves of samples tested at RT and 550 °C under different strain amplitudes (*i.e.*, 0.3%, 0.5% and 0.7(5)%, representing low, medium and high strain amplitudes, respectively). At RT, CoCrFeMnNi in general shows initially cyclic hardening followed by cyclic softening and/or near-steady state until failure (see Fig. 1a). At 550 °C, the material generally exhibits cyclic hardening followed by a near-steady state until failure, except for only near-steady state at low strain amplitudes (≤ 0.3%, see Fig. 1a).

In addition, Fig. 1b, c and d display the hysteresis loops of several typical cycles at strain amplitude of 0.3%, 0.5% and 0.7(5)% respectively, at both RT and 550 °C. Evidently, in contrast to continuous plastic flow at RT, serrated plastic flow is initially observed under medium-to-high strain amplitudes (0.5% and 0.75%) at 550 °C, see Fig. 1c-d. However, upon further cycling, serrations magnitude decreases and finally tends to be zero (Fig. 1c-d). Notably, the serrated flow was not observed at 550 °C under low strain amplitude (*e.g.*, 0.3%, Fig. 1b), which may be due to limited data points at the plastic deformation stage. Together, these results reveal a temperature-dependent cyclic stress response. In comparison to RT, the main differences at 550 °C lie in the absence of cyclic softening and the presence of serrated plastic flow.

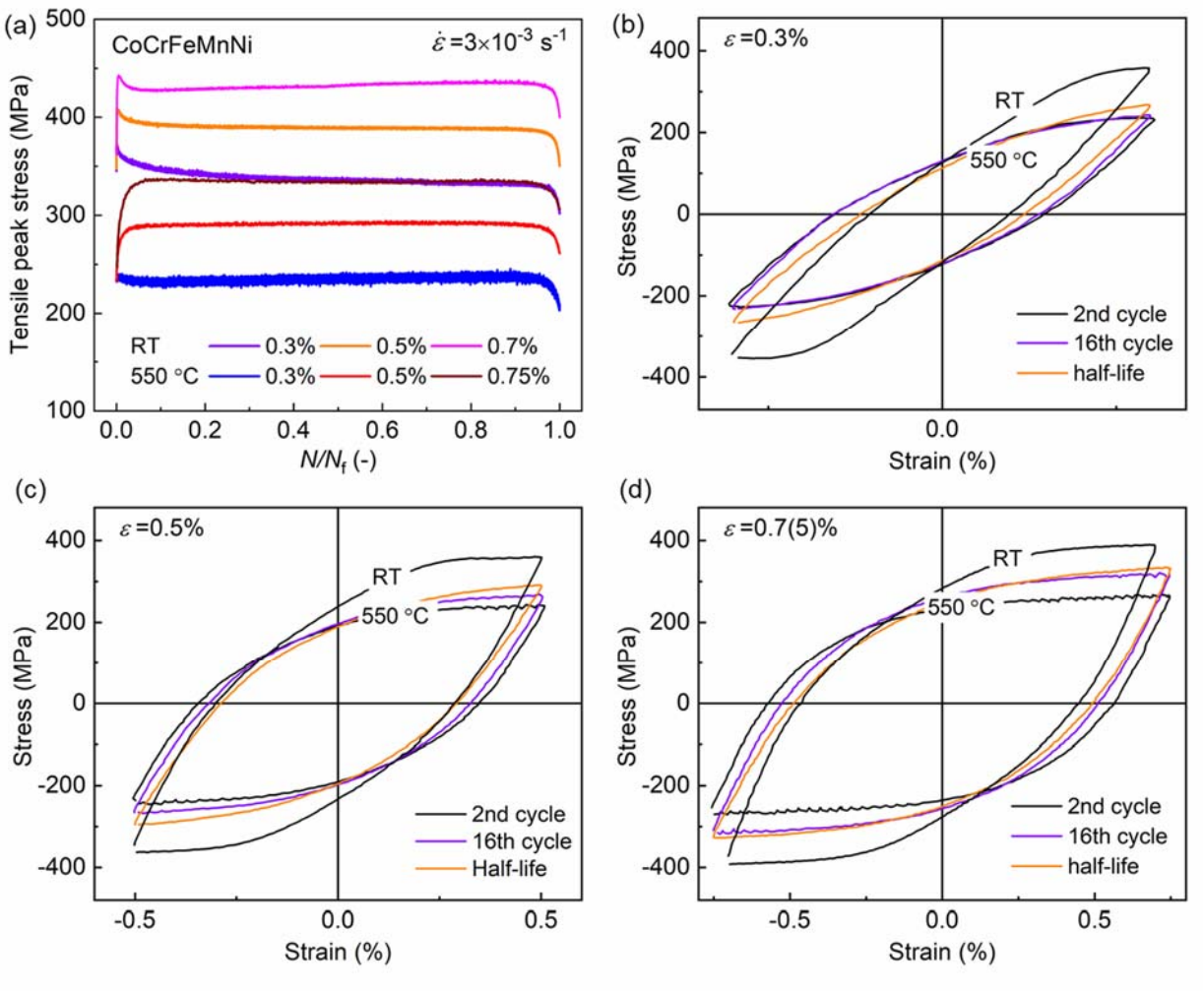


Fig. 1. Comparison of (a) cyclic stress response, as well as (b-d) hysteresis loops of several cycles at strain amplitude of 0.3%, 0.5% and 0.7(5)%, respectively, for CoCrFeMnNi tested at RT and 550 °C. (b-d) include results at the 2nd cycle for RT, as well as at the 2nd, 16th and half-life cycles for 550 °C.

Furthermore, by plotting the saturated stress amplitude *versus* inelastic strain amplitude (obtained from half-life cycles at different strain amplitudes), the cyclic stress-strain relationship can be presented in Fig. 2. This relationship can be fitted by an empirical power-law relation ($\Delta\sigma/2 = K'(\Delta\varepsilon_{\mathrm{in}}/2)^{n'}$ [19], where $K'$ is the cyclic strength coefficient and $n'$ is the cyclic work hardening exponent). The fitted curves/parameters are also given in Fig. 2. Clearly, the slope of the curve (*i.e.*, $n'$ value) at 550 °C (of 0.14) is lower than that at RT (of 0.19). As suggested in Refs. [20, 21], the noticeable difference in $n'$ value of different FCC alloys could reflect their different slip modes. Therefore, if this empirical law is valid for HEAs, different dislocation slip modes could be anticipated at different temperatures. This will be confirmed later by TEM investigations.

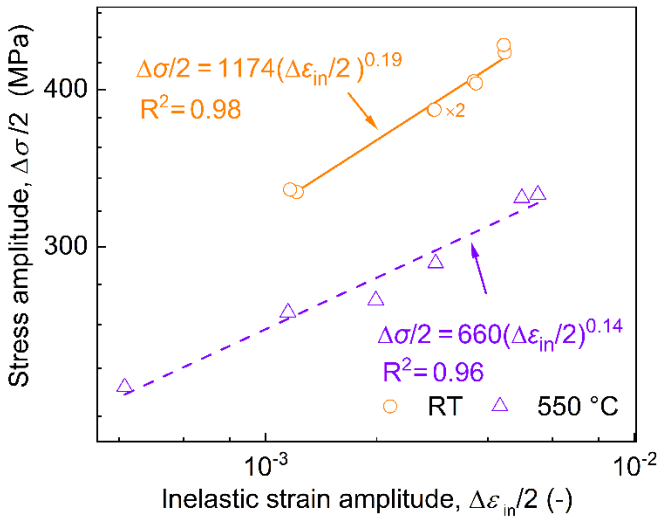


Fig. 2. Comparisons of cyclic stress-strain relationship for CoCrFeMnNi tested at RT and 550 °C.

The temperature influence on the fatigue life is analyzed by plotting the Manson-Coffin curves ($\Delta\varepsilon_{\mathrm{in}}/2 = \varepsilon'_{\mathrm{f}}(2N_{\mathrm{f}})^{c}$ [22, 23]) and Wöhler curves, see Fig. 3a and b, respectively. The comparison shows that, under similar strain and stress conditions, the lifetime is shorter at 550 °C than that at RT (Fig. 3).

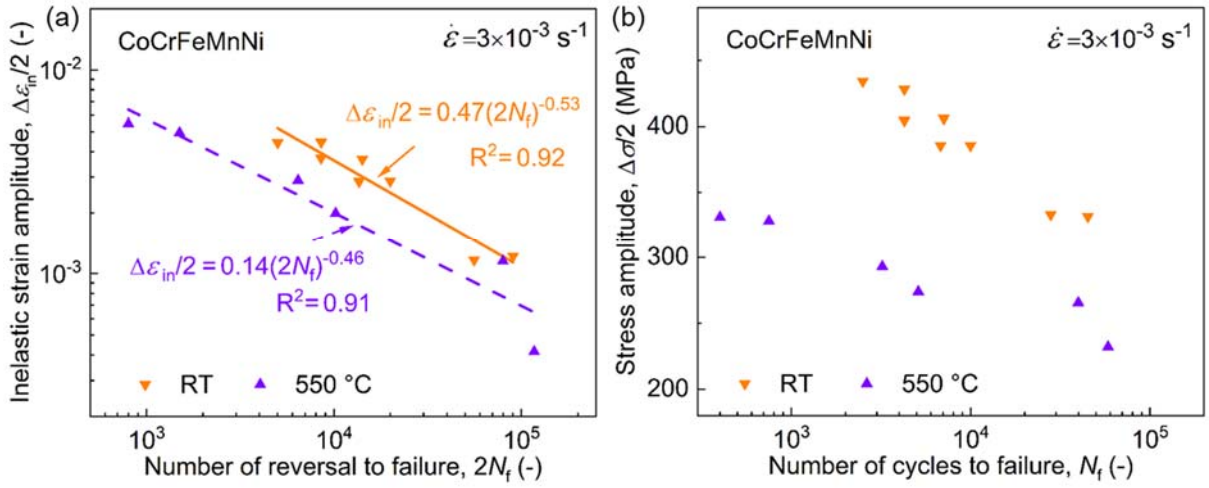


Fig. 3. Comparisons of (a) Manson-Coffin plot and (b) Wöhler plot for CoCrFeMnNi tested at RT and 550 °C.

To uncover the reasons for the difference in the cyclic stress response and lifetime at RT and 550 °C, the microstructures of post-fatigued samples were characterized by TEM. As discussed in detail in Ref. [5], at RT, increasing strain amplitude from 0.3% to 0.5% leads to the transition of dislocation structures from planar configurations (*i.e.*, slip bands, SBs) to pronounced wavy substructures (*e.g.*, walls and cells), *e.g.*, see

Fig. 4. This transition is mainly related to the activation of multiple-slip and cross-slip at higher strain amplitudes [5].

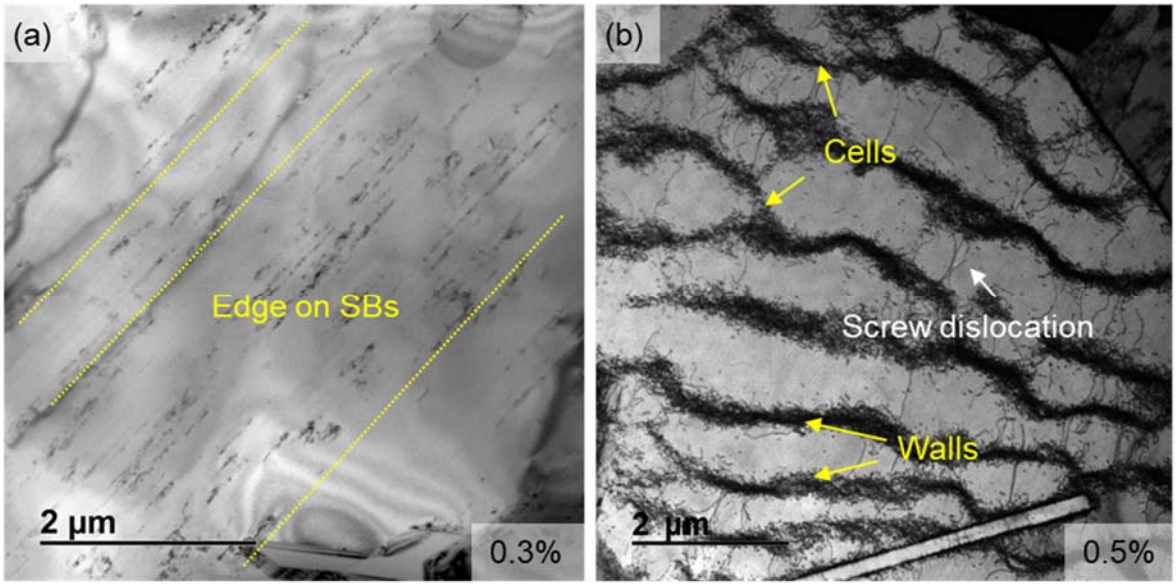


Fig. 4 Typical dislocation structures formed in post-fatigued CoCrFeMnNi samples tested at RT under a (a) low, 0.3%, and (b) medium, 0.5% strain amplitude.

Typical microstructures in post-fatigued CoCrFeMnNi samples at 550 °C and different strain amplitudes are shown in Fig. 5. On one hand, at low strain amplitudes (*i.e.*, 0.2% and 0.3%), most grains manifest low density of planar SBs and discrete dislocations (see Fig. 5a-b). This observation indicates prevalent planar slip, which is similar to that at RT under low strain amplitude (see Fig. 4a).

On the other hand, at 550 °C and medium-to-high strain amplitudes (0.5% and 0.75%), both dislocation substructures (*e.g.*, walls separated by channels) and tangles are recognized (Fig. 5c-f). Among them, the substructures formation at 550 °C (Fig. 5d, f) is analogous to the main wavy features at RT (Fig. 4b), indicating multiple slip and wavy slip activation. Nevertheless, the tangles are distinct from the main wavy features at RT. This is because they are found to consist of partial dislocations with in-between SFs (Fig. 5e), suggesting active planar slip.

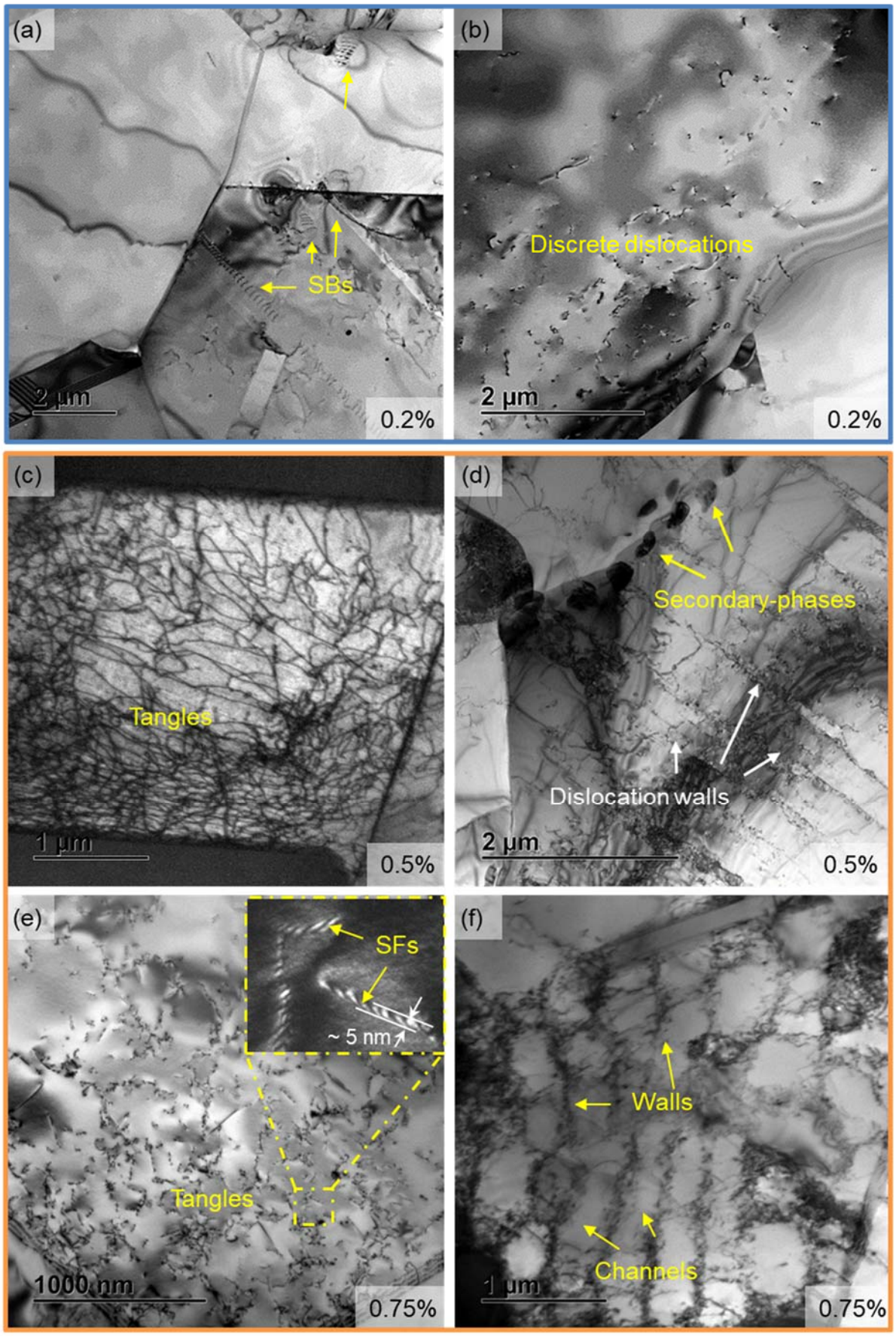


Fig. 5. Typical dislocation structures observed in CoCrFeMnNi samples tested at 550 °C and (a-b) 0.2%, (c-d) 0.5% as well as (e-f) 0.75% strain amplitude. All figures are bright-field

TEM micrographs, except for a weak-beam dark-fried micrograph in the inset of (e) illustrating partial dislocations with in-between stacking faults (SFs). The SF width in the inset of (e) is estimated to be ~ 5 nm. (d) is reproduced here from Ref. [6].

In comparison to RT, the coexisting planar slip (*i.e.*, tangles) at 550 °C suggests a reduced extent of wavy substructures formation (*i.e.*, dynamic recovery). In other words, the propensity of dynamic recovery is lower at 550 °C as compared to RT. This can be further supported by the higher EBSD-based KAM values at 550 °C as than that at RT (see Fig. 6a-b, indicated by more green data points in (b) than that in (a)). The higher KAM values represent higher GND densities at 550 °C than that at RT, consistent with the observation in [24].

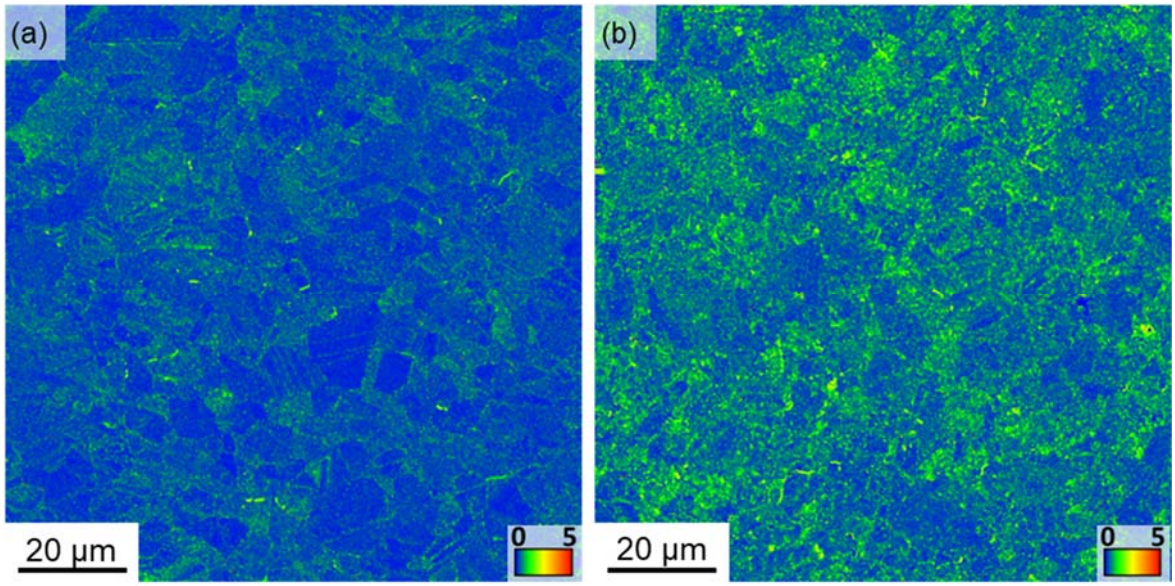


Fig. 6. KAM maps acquired from EBSD scanning for CoCrFeMnNi samples tested under 0.5% strain amplitude at (a) RT and (b) 550 °C. The average KAM values at 550 °C (b) are higher than those at RT(a), indicated by more green data points in (b).

## 4. Discussion

### 4.1. Evolution of deformation mode

Based on TEM analyses, this study reveals dislocation's slip mode evolution with strain amplitude and cycle number at 550 °C, as illustrated in Fig. 7. The results at RT are also included for later comparison.

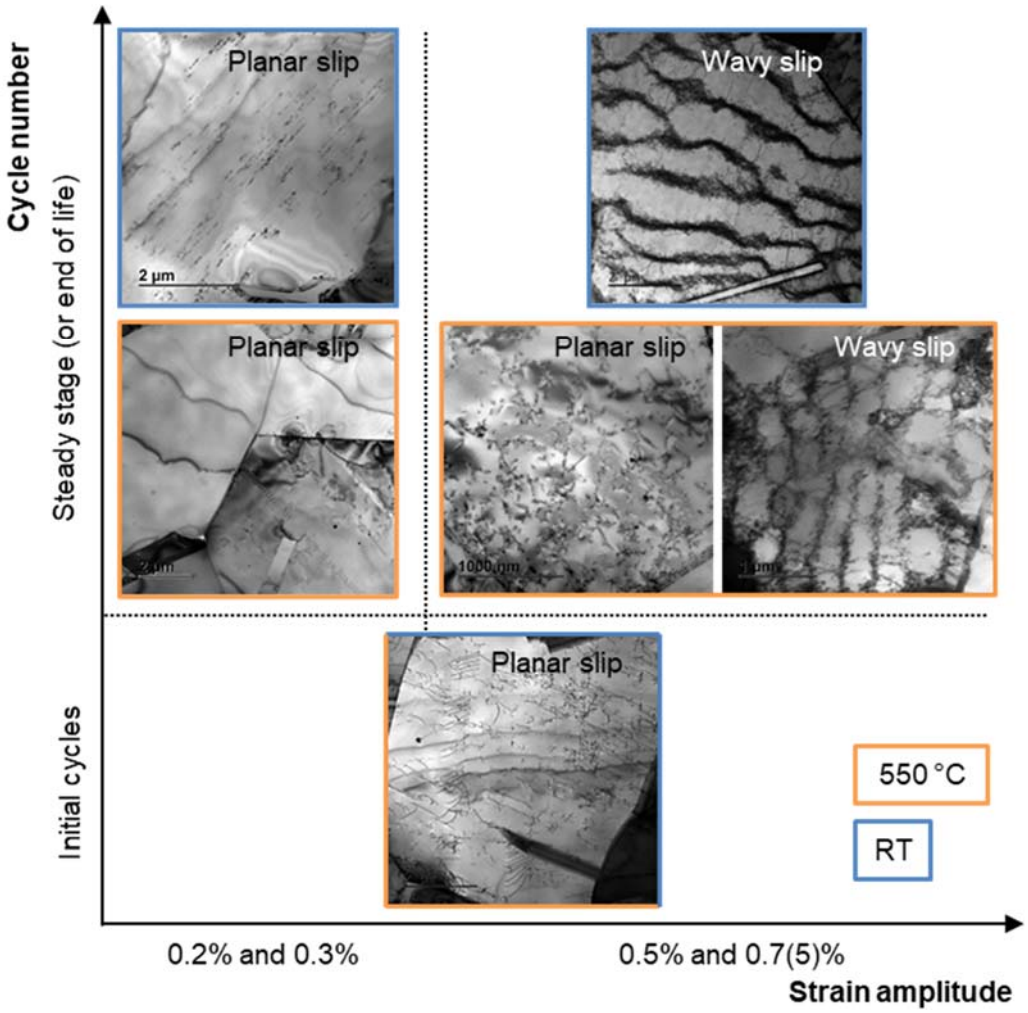


Fig. 7. Schematic illustration of dislocation slip mode evolution with strain amplitude, cycle number and temperature. The planar slip at initial cycles is valid for both RT and 550 °C.

Firstly, the prevalent planar slip was recognized during initial cycles at different temperatures [5, 15]. Along with the current TEM observations, it can be concluded that: at 550 °C, with increasing cycle number, under low strain amplitudes (0.2% and 0.3%), the slip mode remains planar slip; whereas, under medium-to-high strain amplitudes (0.5% and 0.75%), it changes from initially planar slip to coexisting planar slip and wavy slip (Fig. 7). These findings complement our previous report on the evolution of dislocation density upon cycling at 550 °C [6]. As the deformation mode of FCC ductile materials is primarily determined by the stacking fault energy (SFE) [3], the above evolution of slip mode is also believed to be applicable for other FCC HEAs and conventional steels of similar SFE.

By comparing the microstructural features between RT (Fig. 4) and 550°C (Fig. 5), this work also demonstrates the temperature influence on the operating cyclic slip mode. The main difference is observed at the near-steady (or end of life) under medium-to-

high strain amplitudes (0.5% and 0.75%), see Fig. 7. At these conditions, in contrast to the dominating wavy slip at RT, planar slip complements the wavy slip at 550 °C. This confirms the prediction of their different slip mode from the cyclic stress-strain curves (Fig. 2).

### 4.2. Reasons for deformation mode at 550 °C

At 550 °C, under low strain amplitudes, the dominating planar slip can be explained by limited activated slip system at lower stresses. While under medium-to-high strain amplitudes, the presence of wavy slip is expected, and is mainly associated with the thermal recovery and stress-induced activation of cross slip at higher stresses [6]. However, the co-existing planar slip at higher strain amplitudes is rather unanticipated. This might be rationalized by the well-known Suzuki segregation [25], which is believed to increase dislocations disassociation width (or SF width) [26, 27]. Direct evidence on Suzuki segregation has been reported for stainless steels, Ni- and Co-Ni- based superalloys [27-31]. For example, in a stainless steel, the SF width deformed at elevated temperatures is larger than that at RT [28]. Furthermore, in Ni-based superalloys, the segregation of Co and Cr at the SF at 750 °C was observed using Super-X energy-dispersive X-ray spectroscopy (EDS) [29].

In this study, upon cycling CoCrFeMnNi HEA at 550 °C, development of MnNi- and Cr-enriched secondary phases is observed along grain boundaries (*e.g.*, see Fig. 5d, detailed EDS mapping see Ref. [6]), suggesting elemental diffusion. Recently, for a pre-deformed CoCrFeMnNi followed by annealing at 800 °C for 30 min, slight enrichment of Mn element at the SF was observed [16]. In this context, the elemental diffusion generated second phases in our study could be taken as an indication of possible segregation of solutes to SF. This segregation may give rise to high energy barriers for Shockley partials constriction and increase the SF width. The evidence of increased SF width at 550 °C can be found in Fig. 5e (~ 5 nm), as compared to a full screw dislocation at RT in Fig. 4b. Therefore, Suzuki segregation is suggested to play a role upon cycling CoCrFeMnNi at elevated temperatures, provided that the temperature is high enough to allow atomic diffusion to occur at a speed comparable to that of the dislocations [16]. Nevertheless, more efforts are required to provide direct evidence of Suzuki segregation and understand the corresponding driving force for CoCrFeMnNi.

It is also worth noting that, the presence of planar slip (or wavy slip) in different grains under medium-to-high strain amplitudes at 550 °C could be associated with (1) grain orientation and (2) constraints by neighboring grains. These factors might determine the velocity of dislocation motion, and favor the further extension (or constriction) of partial dislocations, leading to planar slip (or wavy slip) in different grains.

### 4.3. Relation of deformation mode with cyclic stress response at 550 °C

The presence of planar slip can be linked with the observed serrated flow in CoCrFeMnNi at 550 °C (Fig. 1c-d). Usually, the serrated flow at elevated temperatures is interpreted by dynamic strain aging behavior, *i.e.*, pinning and de-pinning of planar dislocations by solutes [6, 32, 33]. Similar to the current work, several LCF studies on FCC steels [34-37] rationalized the serrated flow by the dominance of planar slip in similar testing temperature regimes (*e.g.*, 550 °C - 600 °C). Interestingly, unlike the prevalent planar slip in FCC steels, our results reveal that in CoCrFeMnNi, dislocations wavy slip complements planar slip after several cycles cycling at 550 °C (see Fig. 7). Moreover, this following onset of wavy slip might contribute to the gradually disappearing serrated flow at 550 °C (Fig. 1c-d). Therefore, this work suggests that, upon cycling FCC materials at intermediate elevated temperatures (*e.g.*, 550 °C), the role of wavy slip (*e.g.*, probably to reduce the magnitude of serrated flow) should not be neglected (or should be interpreted with caution).

Additionally, the dislocation slip behavior can be associated with the presence or absence of cyclic softening at different temperatures. At RT, the cyclic softening has been correlated to the pronounced dislocation wavy substructures formation, due to increased mean free path for mobile dislocations [3, 5]. Differently, at 550 °C, the extent of wavy substructures formation has been reduced because of coexisting planar slip, which could be responsible for the limited cyclic softening herein (Fig. 1a).

### 4.4. Fatigue life

The reasons for the different lifetime at two investigated temperatures should be clarified. At RT, dislocation's wavy slip induced strain localization plays a significant role in cracks initiation (*i.e.*, by forming intrusions and extrusions). Compared to extensive wavy substructures formation at RT (Fig. 4b), dislocation planar configurations (*e.g.*, tangles) at 550 °C indicate that, the deformation herein is more

homogeneously distributed (*i.e.*, less localized). However, despite less localized deformation, the lifetime is shorter at 550 °C compared to RT for the same inelastic strain amplitudes (Fig. 3a). From the microstructure perspective, these observations suggest that other factors contribute to the shorter lifetime at 550 °C.

One of the factors could be the elemental segregation induced secondary phases (*i.e.*, Cr- and MnNi-enriched phases, Fig. 5d) formation along grain boundaries. Once connected with surface grains, they may not only act as cracks initiation sites but also accelerate cracks propagation, leading to earlier failure. Another factor negatively affecting the lifetime is the *in-situ* high-temperature oxidation, which is known to shorten the fatigue life of materials [7, 9, 35, 36, 38]. Indeed, the oxides layer was observed forming on our fatigued CoCrFeMnNi samples surface [6]. Besides, Polak et al. [38] observed early intergranular cracking and oxidation of grain boundaries during high-temperature cyclic straining, which might also occur in the current material.

## 5. Summary

This study demonstrates the cyclic slip mode evolution of CoCrFeMnNi model HEA at 550 °C. With increasing cycle number, the slip mode remains planar slip at low strain amplitudes (0.2% and 0.3%); whereas, it changes from initially planar slip to coexisting planar slip and wavy slip at medium-to-high strain amplitudes (0.5% and 0.75%).

Furthermore, this work showcases temperature influence on the cyclic deformation behavior of CoCrFeMnNi HEA. In comparison to that at RT, the cyclic response of CoCrFeMnNi shows the absence of cyclic softening and the presence of serrated flow at 550 °C. This can be rationalized by their distinct slip modes. Specifically, in contrast to the dominating wavy slip at RT, dislocations planar slip complements wavy slip at 550 °C. The unexpected planar slip at 550 °C is ascribed to the local increase of stacking fault width, likely due to Suzuki segregation.

Lastly, despite less localized deformation arising from planar slip, CoCrFeMnNi exhibits reduced LCF life at 550 °C. This is linked to elemental segregation and *in-situ* oxidation induced grain boundary embrittlement at 550 °C.

Thus, the present work can also serve as a reference for understanding the temperature-dependent cyclic deformation behavior of other FCC HEAs (and conventional steels) with similar stacking fault energy.

## Acknowledgment

The authors gratefully acknowledge Prof. Dr. M. Heilmaier, Dr. A. Kauffmann, and Dr. A. S. Tirunilai for their helpful comments on this work and for providing the investigated material, as well as Prof. Dr. J. Freudenberger for performing rotary-swaging for the material.

## References

[1] A.G. Wang, X.H. An, J. Gu, X.G. Wang, L.L. Li, W.L. Li, M. Song, Q.Q. Duan, Z.F. Zhang, X.Z. Liao, Effect of grain size on fatigue cracking at twin boundaries in a CoCrFeMnNi high-entropy alloy, Journal of Materials Science & Technology, (2019).

[2] S.A.A. Shams, G. Jang, J.W. Won, J.W. Bae, H. Jin, H.S. Kim, C.S. Lee, Low-cycle fatigue properties of CoCrFeMnNi high-entropy alloy compared with its conventional counterparts, Materials Science and Engineering: A, 792 (2020) 139661.

[3] K. Lu, A. Chauhan, M. Walter, A.S. Tirunilai, M. Schneider, G. Laplanche, J. Freudenberger, A. Kauffmann, M. Heilmaier, J. Aktaa, Superior low-cycle fatigue properties of CoCrNi compared to CoCrFeMnNi, Scripta Materialia, 194 (2021) 113667.

[4] S. Picak, T. Wegener, S.V. Sajadifar, C. Sobrero, J. Richter, H. Kim, T. Niendorf, I. Karaman, On the Low Cycle Fatigue Response of CoCrNiFeMn High Entropy Alloy with Ultra-fine Grain Structure, Acta Materialia, (2020) 116540.

[5] K. Lu, A. Chauhan, A.S. Tirunilai, J. Freudenberger, A. Kauffmann, M. Heilmaier, J. Aktaa, Deformation mechanisms of CoCrFeMnNi high-entropy alloy under low-cycle-fatigue loading, Acta Materialia, 215 (2021) 117089.

[6] K. Lu, A. Chauhan, D. Litvinov, M. Walter, A.S. Tirunilai, J. Freudenberger, A. Kauffmann, M. Heilmaier, J. Aktaa, High-temperature low cycle fatigue behavior of an equiatomic CoCrFeMnNi high-entropy alloy, Materials Science and Engineering: A, 791 (2020) 139781.

[7] A. Chauhan, D. Litvinov, J. Aktaa, Deformation and damage mechanisms of a bimodal 12Cr-ODS steel under high-temperature cyclic loading, International Journal of Fatigue, 93 (2016) 1-17.

[8] B. Li, Y. Zheng, J. Zhao, S. Shi, Z. Zhang, X. Chen, Cyclic Deformation Behavior and Dynamic Strain Aging of 316LN Stainless Steel under Low Cycle Fatigue Loadings at 550°C, Materials Science and Engineering: A, (2021).

[9] A. Chauhan, J. Hoffmann, D. Litvinov, J. Aktaa, High-temperature low-cycle fatigue behavior of a 9Cr-ODS steel: Part 1 - pure fatigue, microstructure evolution and damage characteristics, Materials Science and Engineering: A, 707 (2017) 207-220.

[10] W.-M. Choi, S. Jung, Y.H. Jo, S. Lee, B.-J. Lee, Design of new face-centered cubic high entropy alloys by thermodynamic calculation, Metals and Materials International, 23 (2017) 839-847.

[11] M. Heczko, V. Mazánová, C.E. Slone, M. Shih, E.P. George, M. Ghazisaeidi, J. Polák, M.J. Mills, Role of deformation twinning in fatigue of CrCoNi medium-entropy alloy at room temperature, Scripta Materialia, 202 (2021).

[12] C.W. Shao, P. Zhang, R. Liu, Z.J. Zhang, J.C. Pang, Z.F. Zhang, Low-cycle and extremely-low-cycle fatigue behaviors of high-Mn austenitic TRIP/TWIP alloys: Property evaluation, damage mechanisms and life prediction, Acta Materialia, 103 (2016) 781-795.

[13] P. Li, S. Li, Z. Wang, Z. Zhang, Fundamental factors on formation mechanism of dislocation arrangements in cyclically deformed fcc single crystals, Progress in Materials Science, 56 (2011) 328-377.

[14] M.S. Pham, S.R. Holdsworth, K.G.F. Janssens, E. Mazza, Cyclic deformation response of AISI 316L at room temperature: Mechanical behaviour, microstructural evolution, physically-based evolutionary constitutive modelling, International Journal of Plasticity, 47 (2013) 143-164.

[15] F. Otto, A. Dlouhý, C. Somsen, H. Bei, G. Eggeler, E.P. George, The influences of temperature and microstructure on the tensile properties of a CoCrFeMnNi high-entropy alloy, Acta Materialia, 61 (2013) 5743-5755.

[16] M. Kawamura, M. Asakura, N.L. Okamoto, K. Kishida, H. Inui, E.P. George, Plastic deformation of single crystals of the equiatomic Cr−Mn−Fe−Co−Ni high-entropy alloy in tension and compression from 10 K to 1273 K, Acta Materialia, 203 (2021).

[17] M. Zhang, E.P. George, J.C. Gibeling, Elevated-temperature Deformation Mechanisms in a CrMnFeCoNi High-Entropy Alloy, Acta Materialia, (2021) 117181.

[18] M. Calcagnotto, D. Ponge, E. Demir, D. Raabe, Orientation gradients and geometrically necessary dislocations in ultrafine grained dual-phase steels studied by 2D and 3D EBSD, Materials Science and Engineering: A, 527 (2010) 2738-2746.

[19] J. Morrow, Cyclic plastic strain energy and fatigue of metals, in: Internal friction, damping, and cyclic plasticity, ASTM International, 1965.

[20] C.E. Feltner, C. Laird, Cyclic stress-strain response of F.C.C. metals and alloys—I Phenomenological experiments, Acta Metallurgica, 15 (1967) 1621-1632.

[21] D. Han, Y.J. Zhang, X.W. Li, A crucial impact of short-range ordering on the cyclic deformation and damage behavior of face-centered cubic alloys: A case study on Cu-Mn alloys, Acta Materialia, 205 (2021).

[22] S.S. Manson, Behavior of materials under conditions of thermal stress, National Advisory Committee for Aeronautics, 1953.

[23] L. Coffin Jr, A study of the effects of cyclic thermal stresses on a ductile metal, Transactions of the American Society of Mechanical Engineers, New York, 76 (1954) 931-950.

[24] Q. Han, X. Lei, S.-S. Rui, Y. Su, X. Ma, H. Cui, H. Shi, Temperature-dependent fatigue response of a Fe44Mn36Co10Cr10 high entropy alloy: A coupled in-situ electron microscopy study and crystal plasticity simulation, International Journal of Fatigue, 151 (2021).

[25] H. Suzuki, Chemical interaction of solute atoms with dislocations, Sci. Rep. Res. Inst. Tohoku Univ. A, 4 (1952) 455-463.

[26] P. Gallagher, The influence of alloying, temperature, and related effects on the stacking fault energy, Metallurgical Transactions, 1 (1970) 2429-2461.

[27] H. Saka, Experimental evidence for Suzuki segregation to the stacking fault of an extended dislocation in a Cu-Si alloy, Philosophical Magazine A, 47 (1983) 131-140.

[28] Y. Kaneko, K. Kaneko, A. Nohara, H. Saka, Evidence for Suzuki effect in an Fe-Ni-Cr austenitic stainless steel, Philosophical Magazine A, 71 (1995) 399-407.

[29] G.B. Viswanathan, R. Shi, A. Genc, V.A. Vorontsov, L. Kovarik, C.M.F. Rae, M.J. Mills, Segregation at stacking faults within the $\gamma'$ phase of two Ni-base superalloys following intermediate temperature creep, Scripta Materialia, 94 (2015) 5-8.

[30] G.W. Han, I.P. Jones, R.E. Smallman, Direct evidence for Suzuki segregation and Cottrell pinning in MP159 superalloy obtained by FEG(S)TEM/EDX, Acta Materialia, 51 (2003) 2731-2742.

[31] Y. Koizumi, T. Nukaya, S. Suzuki, S. Kurosu, Y. Li, H. Matsumoto, K. Sato, Y. Tanaka, A. Chiba, Suzuki segregation in Co–Ni-based superalloy at 973K: An experimental and computational study by phase-field simulation, Acta Materialia, 60 (2012) 2901-2915.

[32] P. G. McCormick, A model for the Portevin-Le Chatelier effect in substitutional alloys, Acta Metallurgica, 20 (1972) 351-354.

[33] J.X. Fu, C.M. Cao, W. Tong, Y.X. Hao, L.M. Peng, The tensile properties and serrated flow behavior of a thermomechanically treated CoCrFeNiMn high-entropy alloy, Materials Science and Engineering: A, 690 (2017) 418-426.

[34] R. Sandhya, K.B.S. Rao, S. Mannan, R. Devanathan, Substructural recovery in a cold worked Ti-modified austenitic stainless steel during high temperature low cycle fatigue, International journal of fatigue, 23 (2001) 789-797.

[35] D.W. Kim, W.-S. Ryu, J.H. Hong, S.-K. Choi, Effect of nitrogen on high temperature low cycle fatigue behaviors in type 316L stainless steel, Journal of Nuclear Materials, 254 (1998) 226-233.

[36] V.S. Srinivasan, M. Valsan, R. Sandhya, K. Bhanu Sankara Rao, S.L. Mannan, D.H. Sastry, High temperature time-dependent low cycle fatigue behaviour of a type 316L(N) stainless steel, International Journal of Fatigue, 21 (1999) 11-21.

[37] S.-G. Hong, S.-B. Lee, Mechanism of dynamic strain aging and characterization of its effect on the low-cycle fatigue behavior in type 316L stainless steel, Journal of Nuclear Materials, 340 (2005) 307-314.

[38] J. Polák, R. Petráš, M. Heczko, I. Kuběna, T. Kruml, G. Chai, Low cycle fatigue behavior of Sanicro25 steel at room and at elevated temperature, Materials Science and Engineering: A, 615 (2014) 175-182.